LETTER

doi:10.1038/nature20556

Zika virus infection damages the testes in mice

Jennifer Govero[1]*, Prabagaran Esakky[2]*, Suzanne M. Scheaffer[2], Estefania Fernandez[3], Andrea Drury[2], Derek J. Platt[4], Matthew J. Gorman[3], Justin M. Richner[1], Elizabeth A. Caine[1], Vanessa Salazar[1], Kelle H. Moley[2,5] & Michael S. Diamond[1,3,4,6]

Infection of pregnant women with Zika virus (ZIKV) can cause congenital malformations including microcephaly, which has focused global attention on this emerging pathogen[1]. In addition to transmission by mosquitoes, ZIKV can be detected in the seminal fluid of affected males for extended periods of time and transmitted sexually[2]. Here, using a mouse-adapted African ZIKV strain (Dakar 41519), we evaluated the consequences of infection in the male reproductive tract of mice. We observed persistence of ZIKV, but not the closely related dengue virus (DENV), in the testis and epididymis of male mice, and this was associated with tissue injury that caused diminished testosterone and inhibin B levels and oligospermia. ZIKV preferentially infected spermatogonia, primary spermatocytes and Sertoli cells in the testis, resulting in cell death and destruction of the seminiferous tubules. Less damage was caused by a contemporary Asian ZIKV strain (H/PF/2013), in part because this virus replicates less efficiently in mice. The extent to which these observations in mice translate to humans remains unclear, but longitudinal studies of sperm function and viability in ZIKV-infected humans seem warranted.

We and others have observed that infection of male adult mice with ZIKV results in infection of the testes[3,4], which is consistent with observed male-to-female[5,6] and male-to-male[7] sexual transmission in humans. To address the effects of infection on the male reproductive tract, we performed a longitudinal study in wild-type C57BL/6 mice infected with ZIKV (strains H/PF/2013 (French Polynesia 2013) or mouse-adapted Dakar 41519 (Senegal 1984)) or DENV (serotype 2, strain D2S20). Because ZIKV and DENV do not efficiently antagonize type I interferon (IFN) signalling in mice compared to humans[8], animals were treated with a single dose of IFNα and IFNβ receptor 1 (Ifnar1)–blocking monoclonal antibody to facilitate infection and dissemination. When wild-type mice were treated with an isotype-control antibody instead and then infected, ZIKV RNA did not accumulate in the testes (Fig. 1a).

In the presence of the anti-Ifnar1 antibody, high levels of viral RNA (10^5–10^8 focus-forming unit (FFU) equivalents per g or ml) and infectious virus (up to 10^8 plaque-forming units (PFU) per g or ml) were detected in the testis, epididymis and the fluid collected from the epididymis within seven days of infection with either of the two ZIKV strains but not DENV (Fig. 1a–c). ZIKV-Dakar replicated to higher levels than ZIKV-H/PF/2013, which is consistent with the enhanced virulence of ZIKV-Dakar in wild-type mice[3]. Notably, ZIKV RNA and infectious virus were also detected in mature sperm collected from the epididymis (Fig. 1b, c, and Extended Data Fig. 1). At day 7 after inoculation, ZIKV-infected testes appeared similar in size to uninfected testes from age-matched mice and had equivalent weights (Fig. 1d, e). Histological analysis of ZIKV-infected testis and epididymis at day 7 revealed no apparent differences in architecture (Fig. 1f and Extended Data Fig. 2). However, staining for CD45 (a pan-leukocyte marker) was observed in testis sections only from ZIKV-infected animals, with $CD45^+$ cells localizing to the interstitium between the seminiferous tubules (Fig. 1g, column 1). The blood–testis barrier (BTB) remained intact at day 7 after infection, as shown by equivalent staining of the ETV5 transcription factor (which mediates BTB function and testicular immune privilege[9]) in Sertoli and germ cells in sections from uninfected and ZIKV-infected mice (Fig. 1g, column 2). Furthermore, there was no CD45 staining on the seminiferous tubular side of the BTB, near the $TRA98^+$ germ cells or spermatogonia (Fig. 1g, column 1). A similar pattern of CD45 staining in the testicular interstitium and epididymal epithelium was described in patients infected with HIV[10]; indeed, we also observed scattered $CD45^+$ cells in the epididymal epithelium of ZIKV-infected mice (Fig. 1g, column 5). However, at day 7, $F4/80^+$ macrophages were not apparent in the testicular interstitium or the lumenal epithelium of the epididymis of ZIKV-infected mice (Fig. 1g, columns 3 and 4).

To determine which cells were targeted by ZIKV, we performed *in situ* hybridization (ISH) for viral RNA at day 7 after infection. In the testis, ZIKV RNA was evident in spermatogonia, primary spermatocytes and the trophic, inhibin B-producing Sertoli cells (Fig. 1h, left), with relative sparing of the androgen-producing Leydig cells. In the cauda epididymis, mature sperm in the lumen stained strongly for ZIKV RNA (Fig. 1h, right) as did sperm cells collected from the epididymis (Extended Data Fig. 1).

We followed the consequences of ZIKV infection of the male reproductive tract over time. At day 14 after inoculation, high levels of ZIKV RNA persisted in the testis, epididymis, the fluid from the epididymis and mature sperm of most mice (Fig. 2a). In ZIKV-Dakar-infected animals, there was a noticeable decrease in testis size and weight (Fig. 2b, c). In comparison, no noticeable infection by DENV was observed in the testis at this time point (Extended Data Fig. 3a). Histological analysis of the ZIKV-infected testis at day 14 showed damage to the architecture of the seminiferous tubules with loss of the central ductal lumen (Fig. 2d). This was associated with decreased numbers of $TRA98^+$ germ cells and $Lina28a^+$ type A and B spermatogonia, morphological abnormalities of $GATA4^+$ Sertoli cells and detachment of Sertoli cells from the basement membrane (Fig. 2e and Extended Data Fig. 2). In some regions, large numbers of $CD45^+$ leukocytes were observed, suggesting substantial inflammatory cell infiltration (Fig. 2d, left; e, column 1). The absence of $ETV5^+$ cells at this time point indicates loss of integrity of the BTB, which could explain the extent of interstitial inflammation and $F4/80^+$ macrophages in the affected testis. The epididymis of ZIKV-infected animals also showed tissue injury at day 14, as indicated by constriction of the epididymal lumen, thickening of inter-luminal tissue and accumulation of sperm interspersed with necrotic bodies (Fig. 2d, e, right). ISH at day 14 showed progressive evidence of ZIKV RNA in cells of the testis, in the mature lumenal sperm and on cilia layering the inner lumen of the epididymis, similar to day 7 (Fig. 2f).

High levels of viral RNA persisted in tissues of the male reproductive tract at 21 days after ZIKV-Dakar inoculation (Fig. 3a), and this

[1]Department of Medicine, Washington University School of Medicine, Saint Louis, Missouri 63110, USA. [2]Department of Obstetrics and Gynecology, Washington University School of Medicine, Saint Louis, Missouri 63110, USA. [3]Department of Pathology and Immunology, Washington University School of Medicine, Saint Louis, Missouri 63110, USA. [4]Department of Molecular Microbiology, Washington University School of Medicine, Saint Louis, Missouri 63110, USA. [5]Department of Cell Biology and Physiology, Washington University School of Medicine, Saint Louis, Missouri 63110, USA. [6]The Center for Human Immunology and Immunotherapy Programs, Washington University School of Medicine, Saint Louis, Missouri 63110, USA.
*These authors contributed equally to this work.

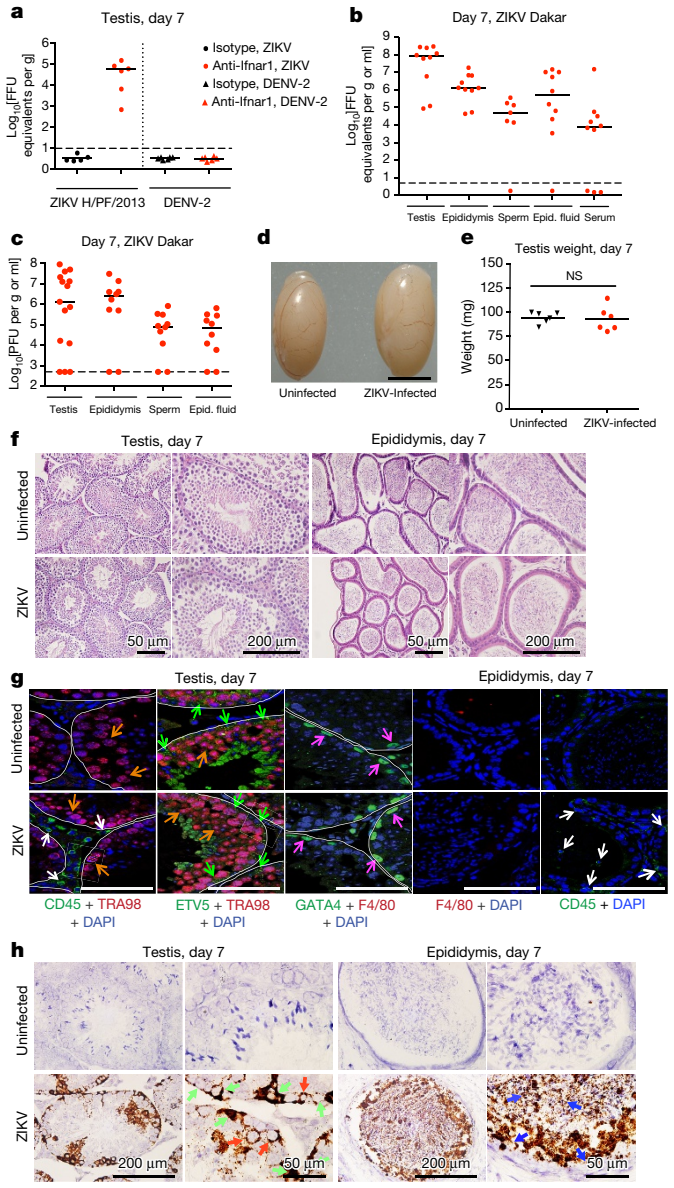

Figure 1 | ZIKV infection of the testis and epididymis at day 7. a–c, Seven-week-old wild-type mice were treated with an isotype control (**a**) or anti-Ifnar1 mouse antibody (2 mg (**a**) or 0.5 mg (**b**, **c**)) at day −1 before subcutaneous inoculation with 10^3 FFU of ZIKV-H/PF/2013 (**a**), 10^6 FFU of DENV-2 (**a**), or 10^6 FFU of mouse-adapted ZIKV-Dakar (**b**, **c**). Tissues and cells were collected at day 7 after infection and analysed for viral RNA by qRT–PCR (**a**, **b**) or for infectious virus by plaque assay (**c**). Dashed lines indicate limit of detection. Results are pooled from two or three independent experiments and each symbol represents data from an individual mouse. Bars indicate median values. Viral RNA was normalized to a standard curve from RNA isolated from infectious virus. **d**, A representative image of testes from uninfected and ZIKV-Dakar-infected mice at day 7; scale bar, 2 mm. **e**, Weight of testes from uninfected and ZIKV-infected mice at day 7. Results are pooled from two independent experiments. Mean values were not statistically different (NS; unpaired *t*-test). **f–h**, Histological, immunohistochemical and ISH analysis of testis (left) and epididymis (right) collected from uninfected or ZIKV-infected animals. **f**, Haematoxylin and eosin staining. **g**, Immunofluorescence staining of uninfected or ZIKV-infected testis and epididymis tissue sections with antibodies to CD45 (pan-leukocyte), TRA98 (germ cells), ETV5 (BTB), GATA4 (Sertoli cells) and F4/80 (macrophages). Arrows indicate staining for leukocytes (white), germ cells (orange), Sertoli cells (magenta) and BTB (green). White lines demarcate tubules of seminiferous epithelium. **h**, ISH with a ZIKV-specific probe. Arrows indicate cells positive for ZIKV RNA (spermatogonia and primary spermatocytes (red), Sertoli cells (green) and epididymis lumenal sperm (blue)). The images in **f–h** are representative of several independent experiments. Scale bars, as indicated (**f**, **h**) and 50 µm (**g**).

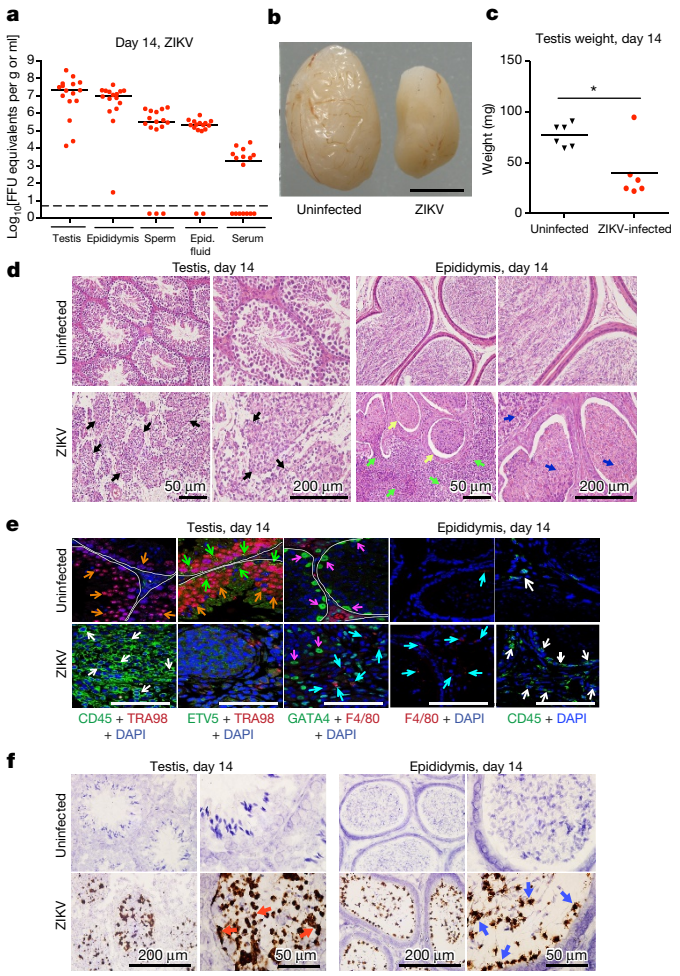

Figure 2 | ZIKV infection of the testis and epididymis at day 14. **a**, **b**, Seven-week-old wild-type mice were treated with 0.5 mg of anti-Ifnar1 at day −1 before subcutaneous inoculation of mouse-adapted ZIKV-Dakar. Tissues and cells were collected at day 14 and analysed for viral RNA by qRT–PCR (**a**). Dashed lines indicate limit of detection. Results are pooled from three independent experiments. Bars indicate median values. **b**, A representative image of testes from uninfected and ZIKV-infected mice at day 14; scale bar, 2 mm. **c**. Weight of testes from uninfected and ZIKV-infected mice at day 14. Results are pooled from two independent experiments (*$P < 0.05$, Mann–Whitney test). **d–f**. Histological, immunohistochemical and ISH analysis of testis (left) and epididymis (right) collected from uninfected or ZIKV-infected animals. **d**, Haematoxylin and eosin staining. Arrows denote involution of seminiferous tubules in the testis (black), constricted epididymal lumens (yellow) with a mass of residual sperm (blue) and thickened epithelium (green). **e**, Immunofluorescence staining of uninfected or ZIKV-infected testis and epididymis tissues as described in Fig. 1. Arrows indicate staining for leukocytes (white), germ cells (orange), Sertoli cells (magenta), BTB (green) and macrophages (cyan). White lines demarcate tubules in the seminiferous epithelium. **f**, ISH. Arrows indicate cells positive for ZIKV RNA (testicular cells (red) and epididymis lumenal sperm and cilia on the inner layer of epididymal epithelium (blue)). The images in **d–f** are representative of several independent experiments. Scale bars, as indicated (**d**, **f**) and 50 µm (**e**).

was associated with a loss of tissue architecture. Involution of the testis was observed, indicated by their noticeably reduced size and weight (Fig. 3b, c). Histological analysis revealed almost complete destruction of the seminiferous epithelium with constricted tubules after ZIKV infection (Fig. 3d). The populations of spermatogonia, Sertoli cells and 3β-HSD$^+$ Leydig cells were markedly diminished, and this was associated with persistent CD45$^+$ leukocyte infiltration (Fig. 3e and Extended Data Fig. 2). In the epididymis, ZIKV infection resulted in constriction of the lumen with a mass of residual sperm that was interspersed

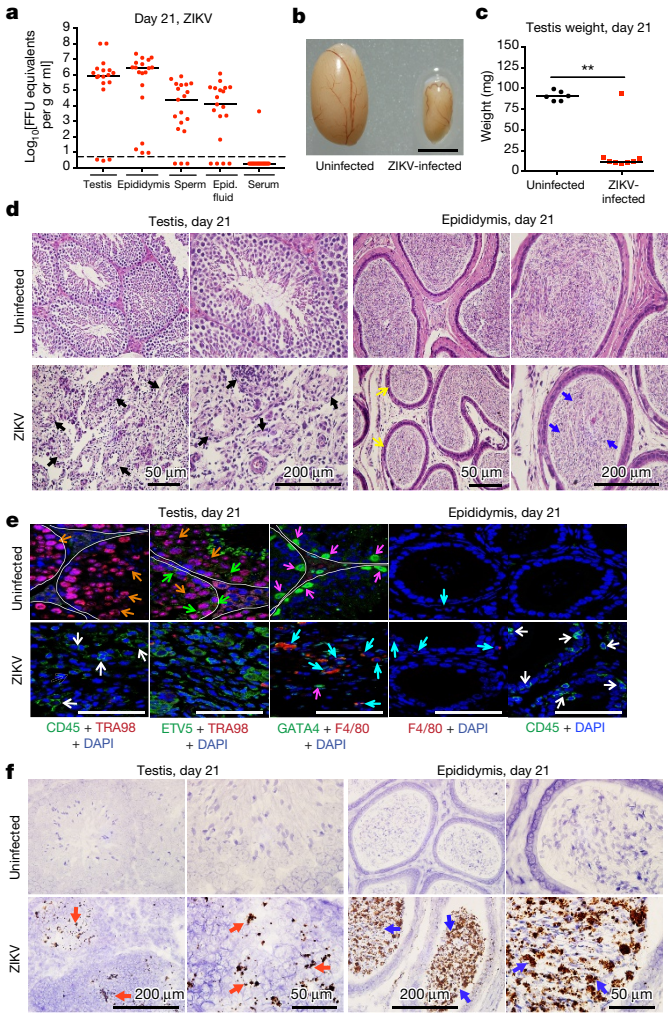

Figure 3 | ZIKV infection of the testis and epididymis at day 21. **a**, Seven-week-old wild-type mice were treated with 0.5 mg of anti-Ifnar1 at day −1 before subcutaneous inoculation of mouse-adapted ZIKV-Dakar. Tissues and cells were collected at day 21 after infection and analysed for viral RNA by qRT–PCR. Dashed lines indicate limit of detection. Results are pooled from two independent experiments. Bars indicate median values. **b**, A representative image of testes from uninfected and ZIKV-infected mice at day 21; scale bar, 2 mm. **c**, Weight of testes from uninfected and ZIKV-infected mice at day 21. Results are pooled from two independent experiments (*$P < 0.05$, Mann–Whitney test). **d**, Histological analysis of testis (left) and epididymis (right) collected from uninfected or ZIKV-infected animals stained with haematoxylin and eosin. Arrows indicate involution of seminiferous tubules in the testis (black), shrunken epididymal lumens (yellow) with a mass of residual sperm (blue). **e**, Immunofluorescence staining of uninfected or ZIKV-infected testis and epididymis tissues as described in Figs. 1, 2. Arrows indicate staining for leukocytes (white), germ cells (orange), Sertoli cells (magenta), BTB (green) and macrophages (cyan). White lines demarcate tubules in the seminiferous epithelium. **f**, ISH. Arrows indicate cells positive for ZIKV RNA (testicular cells (red) and epididymal lumenal sperm (blue)). The images in **d**–**f** are representative of several independent experiments. Scale bars, as indicated (**d**, **f**) and 50 µm (**e**).

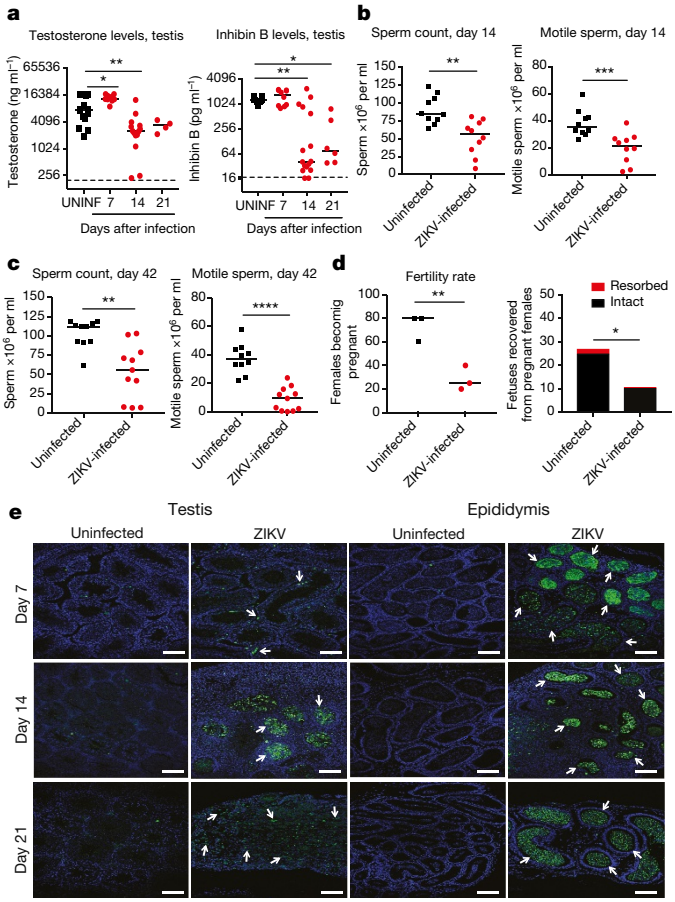

Figure 4 | Consequences of ZIKV infection of the testis and epididymis. **a**, Testosterone (left) and inhibin B (right) levels of testis homogenates from uninfected (UNINF) and ZIKV-infected (days 7, 14 or 21) mice. **b**, **c**, Computer-assisted sperm analysis (total (left) and motile (right)) on samples obtained from the cauda epididymis of ZIKV-infected males immediately after euthanasia at days 14 (**b**) or approximately 42 (41–48 days) (**c**) after infection or age-matched uninfected males. **a**–**c**, Results are pooled from 2–5 independent experiments. Bars indicate median values, and differences between uninfected and ZIKV-infected animals were evaluated (**a**; *$P < 0.05$; **$P < 0.01$; ***$P < 0.001$; ANOVA (Kruskal–Wallis) with a multiple comparison correction; **b**, **c**; **$P < 0.01$; ***$P < 0.001$; ****$P < 0.0001$; Mann–Whitney test). Dashed lines indicate the limit of sensitivity of the assay. **d**, Fertility studies. Age-matched uninfected or ZIKV-infected males (at days 7, 16 or 26 after infection ($n = 4$–5 male mice for each time point)) were mated with individual 8-week-old female wild-type mice ($n = 4$–5 females per round with 3 independent rounds performed) for five days and then separated. Ten days later, we evaluated the pregnancy rate (left, symbols correspond to the percentage of five females becoming pregnant for a given trial) and the total number of viable or resorbed fetuses for each round (right) (*$P < 0.05$; **$P < 0.01$; unpaired Student's *t*-test). **e**, TUNEL staining of testis (left) and epididymis (right) from uninfected or ZIKV-infected mice at days 7, 14 or 21. TUNEL staining in germ and somatic cells of the testis and lumenal sperm in the epididymis is shown (green staining and white arrows). The images are representative of several independent experiments. Scale bars, 100 µm.

with necrotic bodies (Fig. 3d). ISH showed viral RNA in remaining testicular cells of the damaged testis and in the lumenal sperm of the infected epididymis (Fig. 3f). Damage to the seminiferous tubules in the testis, albeit at lower levels, was also observed in mice infected with the epidemic ZIKV-H/PF/2013 strain at day 28 after infection (Extended Data Fig. 3b, c).

The RNA ISH analysis suggested that Sertoli cells were targeted by ZIKV in the testis. Sertoli cells provide a trophic function for spermatogenesis and express high levels of the TAM receptors Tyro3, Axl and Mertk[11]. Because Axl has recently been postulated as an entry factor for ZIKV infection into cells[12–16], we assessed the effect of a genetic deficiency of Axl on ZIKV infection of the testis and epididymis. As we found high levels of infection in the testis and epididymis in $Axl^{-/-}$ mice (Extended Data Fig. 4a), this TAM receptor probably does not have an essential role in ZIKV pathogenesis in the male reproductive tract. ISH showed strong staining of viral RNA in both Sertoli and germ cells in $Axl^{-/-}$ mice at day 7 after ZIKV infection (Extended Data Fig. 4b).

The histological analysis showed that injury of the testis was associated with inflammatory cell infiltration. To assess the role of adaptive immune cells in the pathogenesis of acute disease, we inoculated *Rag1*$^{-/-}$ mice, which lack both mature B and T cells, with ZIKV after a similar treatment with anti-Ifnar1 antibody. At day 7, we observed high levels of viral RNA in all male reproductive tract tissues (Extended Data Fig. 4a). At day 13, we observed ZIKV RNA in germ and Sertoli cells in *Rag1*$^{-/-}$ mice, and this was associated with a decrease in TRA98^{+} germ cells and Lin28a^{+} spermatogonia and breakdown of the BTB. However, interstitial Leydig cells remained in ZIKV-infected *Rag1*$^{-/-}$ mice even though the architecture of the seminiferous tubules was altered (Extended Data Fig. 4c–d). Thus, damage to the testis appears to be mediated both by ZIKV infection and adaptive immune responses.

To determine the functional consequences of ZIKV-Dakar infection in the testis, we measured the levels of two hormones important for spermatogenesis, testosterone and inhibin B, which are produced by Leydig and Sertoli cells, respectively. At day 7 after ZIKV infection, testosterone levels in homogenates of testes were increased, possibly because of the altered cellular physiology or inflammatory environment associated with viral replication[17]. By day 14, testosterone levels in ZIKV-infected mice were decreased and remained low at 21 days (Fig. 4a, left). Inhibin B levels were also reduced in ZIKV-infected testes at days 14 and 21 after infection (Fig. 4a, right). We observed diminished total and motile sperm counts from fluid collected from the cauda epididymis at 14 (Fig. 4b) or approximately 42 (Fig. 4c) days after ZIKV inoculation, which was consistent with extensive damage to the seminiferous tubules (Fig. 2d–f and Extended Data Figs 2, 5a, b). We also observed reduced rates of pregnancy and numbers of viable fetuses from females mated with ZIKV-infected males compared to uninfected males (Fig. 4d). Consistent with substantial injury to the testis, there was marked cell death in the seminiferous tubules and lumen of the epididymis at multiple time points, as indicated by TUNEL staining (Fig. 4e) and loss of cellularity (Fig. 3e, f). Thus, in mice, the injury to the male reproductive tract due to ZIKV infection results in decreased sex hormone production and oligospermia. ZIKV pathogenesis in the testis appears distinct from that of mumps virus, which preferentially infects interstitial Leydig cells and causes highly inflammatory acute orchitis[18,19].

In most human infections, ZIKV causes a mild febrile illness associated with rash and conjunctivitis. However, severe phenotypes are now appreciated, including Guillain-Barré syndrome[20,21] and congenital abnormalities in fetuses[22]. ZIKV can be transmitted sexually, in contrast to related flaviviruses, as infectious virus persists in the semen of males[23–25] for up to 80 days after symptom onset[2]. Our experiments with mouse-adapted ZIKV-Dakar show that infection causes testicular and epididymal damage in mice that can progress to reductions in key sex hormones, destruction of germ and somatic cells in the testis, and loss of mature sperm and fertility. Sertoli cells may be a key target for ZIKV in the testis, resulting in cell dysfunction, detachment from the basement membrane and dissolution of the BTB. Infiltrating inflammatory cells may amplify destruction of the testicular architecture. Although further studies are required, this pathologic process results in decreased male fertility, at least in mice. While Axl is not required for infection of the mouse testis, other TAM or T-cell immunoglobulin and mucin domain (TIM)[15] receptors could be important for ZIKV tropism.

The establishment of a model of male reproductive tract injury after ZIKV infection will allow the rapid testing of new classes of therapeutic agents[26,27] or vaccines[28] to mitigate or prevent disease. Although our data are concerning for yet another unanticipated clinical manifestation of ZIKV infection, we acknowledge these results reflect studies exclusively performed in mice. Nonetheless, genitourinary signs and symptoms, including haematospermia, dysuria and perineal pain[5,6,29], have been reported in ZIKV-infected humans and ZIKV was recently detected in human spermatozoa[30]. Longitudinal studies monitoring ZIKV infection in semen and sperm counts seem warranted to define the extent and consequences of this disease process in affected human males.

Online Content Methods, along with any additional Extended Data display items and Source Data, are available in the online version of the paper; references unique to these sections appear only in the online paper.

Received 23 September; accepted 24 October 2016.
Published online 31 October 2016.

1. Coyne, C. B. & Lazear, H. M. Zika virus—reigniting the TORCH. *Nat. Rev. Microbiol.* **14,** 707–715 (2016).
2. Matheron, S. *et al.* Long-lasting persistence of Zika virus in semen. *Clin. Infect. Dis.* **63,** 1264 (2016).
3. Lazear, H. M. *et al.* A mouse model of Zika virus pathogenesis. *Cell Host Microbe* **19,** 720–730 (2016).
4. Rossi, S. L. *et al.* Characterization of a novel murine model to study Zika virus. *Am. J. Trop. Med. Hyg.* **94,** 1362–1369 (2016).
5. Foy, B. D. *et al.* Probable non-vector-borne transmission of Zika virus, Colorado, USA. *Emerg. Infect. Dis.* **17,** 880–882 (2011).
6. Musso, D. *et al.* Potential sexual transmission of Zika virus. *Emerg. Infect. Dis.* **21,** 359–361 (2015).
7. Deckard, D. T. *et al.* Male–to–Male Sexual Transmission of Zika Virus—Texas, January 2016. *MMWR Morb. Mortal. Wkly. Rep.* **65,** 372–374 (2016).
8. Grant, A. *et al.* Zika virus targets human STAT2 to inhibit type I Interferon signaling. *Cell Host Microbe* **19,** 882–890 (2016).
9. Morrow, C. M. *et al.* ETV5 is required for continuous spermatogenesis in adult mice and may mediate blood testes barrier function and testicular immune privilege. *Ann. NY Acad. Sci.* **1120,** 144–151 (2007).
10. Mullen, T. E. Jr, Kiessling, R. L. & Kiessling, A. A. Tissue-specific populations of leukocytes in semen-producing organs of the normal, hemicastrated, and vasectomized mouse. *AIDS Res. Hum. Retroviruses* **19,** 235–243 (2003).
11. Lu, Q. *et al.* Tyro-3 family receptors are essential regulators of mammalian spermatogenesis. *Nature* **398,** 723–728 (1999).
12. Savidis, G. *et al.* Identification of Zika virus and dengue virus dependency factors using functional genomics. *Cell Reports* **16,** 232–246 (2016).
13. Nowakowski, T. J. *et al.* Expression analysis highlights AXL as a candidate Zika virus entry receptor in neural stem cells. *Cell Stem Cell* **18,** 591–596 (2016).
14. Hamel, R. *et al.* Biology of Zika virus infection in human skin cells. *J. Virol.* **89,** 8880–8896 (2015).
15. Tabata, T. *et al.* Zika virus targets different primary human placental cells, suggesting two routes for vertical transmission. *Cell Host Microbe* **20,** 155–166 (2016).
16. Liu, S., DeLalio, L. J., Isakson, B. E. & Wang, T. T. AXL-Mediated productive infection of human endothelial cells by Zika virus. *Circ. Res.* CIRCRESAHA.116.309866 (2016).
17. Dierich, A. *et al.* Impairing follicle-stimulating hormone (FSH) signaling *in vivo*: targeted disruption of the FSH receptor leads to aberrant gametogenesis and hormonal imbalance. *Proc. Natl Acad. Sci. USA* **95,** 13612–13617 (1998).
18. Wu, H. *et al.* Mumps virus-induced innate immune responses in mouse Sertoli and Leydig cells. *Sci. Rep.* **6,** 19507 (2016).
19. Le Goffic, R. *et al.* Mumps virus decreases testosterone production and gamma interferon-induced protein 10 secretion by human leydig cells. *J. Virol.* **77,** 3297–3300 (2003).
20. Oehler, E. *et al.* Zika virus infection complicated by Guillain-Barre syndrome—case report, French Polynesia, December 2013. *Euro Surveill.* **19,** 20720 (2014).
21. Carteaux, G. *et al.* Zika virus associated with Meningoencephalitis. *N. Engl. J. Med.* **374,** 1595–1596 (2016).
22. Brasil, P. *et al.* Zika virus infection in pregnant women in Rio de Janeiro—preliminary report. *N. Engl. J. Med.* 10.1056/NEJMoa1602412 (2016).
23. Mansuy, J. M. *et al.* Zika virus in semen of a patient returning from a non-epidemic area. *Lancet Infect. Dis.* **16,** 894–895 (2016).
24. Turmel, J. M. *et al.* Late sexual transmission of Zika virus related to persistence in the semen. *Lancet* **387,** 2501 (2016).
25. D'Ortenzio, E. *et al.* Evidence of sexual transmission of Zika virus. *N. Engl. J. Med.* **374,** 2195–2198 (2016).
26. Zhao, H. *et al.* Structural basis of Zika Virus-specific antibody protection. *Cell* **166,** 1016–1027 (2016).
27. Barrows, N. J. *et al.* A Screen of FDA-Approved drugs for inhibitors of Zika virus infection. *Cell Host Microbe* **20,** 259–270 (2016).
28. Larocca, R. A. *et al.* Vaccine protection against Zika virus from Brazil. *Nature* **536,** 474–478 (2016).
29. Torres, J. R., Martinez, N. & Moros, Z. Microhematospermia in acute Zika virus infection. *Int J Infect Dis*, **51,** 127 (2016).
30. Mansuy, J. M. *et al.* Zika virus in semen and spermatozoa. *Lancet Infect. Dis.* **16,** 1106–1107 (2016).

Acknowledgements NIH grants (R01 AI073755 and R01 AI104972 to M.S.D., R01 HD065435 and R01HD083895 to K.H.M., and T32 AI007163 (E.F.)) supported this work. This work was supported by the Washington University Institute of Clinical and Translational Sciences (UL1 TR000448 from the National Center for Advancing Translational Sciences and P41 GM103422-35 from the National Institute of General Medical Sciences to K.H.M.), as well as a grant from the Veteran Affairs Office of Research and Development IO1BX007080 to K.H.M.). The authors thank J. Miner, T. Pierson, P. A. Felder and J. Halabi for technical assistance, manuscript review and data analysis. The testosterone and inhibin B assays were processed by the University of Virginia Center for Research in Reproduction Ligand Assay and Analysis Core, which is supported by the Eunice Kennedy Shriver NICHD/NIH (NCTRI) Grant P50-HD28934.

Author Contributions J.G., P.E., S.M.S., E.F., A.D., D.J.P., J.M.R., E.A.C. and V.S. performed the experiments. M.J.G. provided key reagents. J.G., P.E., S.M.S. and E.F. performed data analysis. M.S.D., P.E. and K.H.M. wrote the initial draft of the manuscript, with all other authors contributing to editing into the final form.

Author Information Reprints and permissions information is available at www.nature.com/reprints. The authors declare competing financial interests: details are available in the online version of the paper. Readers are welcome to comment on the online version of the paper. Correspondence and requests for materials should be addressed to K.H.M. (moleyk@wustl.edu) or M.S.D. (diamond@wusm.wustl.edu).

METHODS

Ethics statement. This study was carried out in accordance with the recommendations in the Guide for the Care and Use of Laboratory Animals of the National Institutes of Health. The protocols were approved by the Institutional Animal Care and Use Committee at the Washington University School of Medicine (Assurance number A3381-01). Inoculations were performed under anaesthesia induced and maintained with ketamine hydrochloride and xylazine, and all efforts were made to minimize animal suffering.

Viruses. ZIKV strain H/PF/2013 (French Polynesia, 2013) was provided by the Arbovirus Branch of the Centers for Disease Control and Prevention with permission (X. de Lamballerie). ZIKV strain Dakar 41519 (Senegal, 1984) was provided by the World Reference Center for Emerging Viruses and Arboviruses (R. Tesh) and passaged twice in *Rag1*$^{-/-}$ mice to create a mouse-adapted, more pathogenic variant of ZIKV-Dakar (M. Gorman and M. Diamond, unpublished results). DENV-2 (strain D2S20) was obtained as a gift (S. Shresta). Virus stocks were propagated in mycoplasma-free Vero cells (ATCC) and titrated by focus-forming assay (FFA), as described previously[3].

Mouse infection experiments. Wild-type C57BL/6 mice were purchased commercially (Jackson Laboratories) and congenic *Rag1*$^{-/-}$ mice were bred at Washington University in a pathogen-free facility. Congenic *Axl*$^{-/-}$ mice were described previously[31]. Seven-week-old mice were inoculated by subcutaneous route in the footpad with 10^3 (H/PF/2013) or 10^6 (Dakar 41519 or DENV-2) FFU in a volume of 50 μl. One-day before inoculation with virus, mice were treated with 0.5 or 2 mg of an Ifnar1-blocking mouse antibody (MAR1-5A3) or isotype control mouse antibody (GIR-208) by intraperitoneal injection[3]. At different days after infection, tissues were collected and processed as described below. Testis and epididymis collected from infected male mice were processed for haematoxylin and eosin staining, immunofluorescence and confocal microscopy, ISH and viral titer analysis as described previously[32]. Testes were also examined macroscopically and weighed. At days 14, 21 and around 42 after ZIKV-Dakar infection, the macroscopic damage as indicated by a reduction in size was often uniformly bilateral, although some asymmetry in testis (right versus left) size was observed. Randomization and blinding of the animal experiments were not performed, and sample sizes were not calculated beforehand.

Computer-assisted sperm analysis (CASA). Mature sperm from the cauda epididymis of uninfected or virus-infected mice were collected immediately after euthanasia as reported earlier[33]. The sperm suspension in vitrofert medium (Cook Medical) was analysed for total sperm count by CASA using the HTM-IVOS Vs12 integrated visual optical system motility analyser (Hamilton-Thorne Research) as described previously[34]. For studies at around 42 day after infection, mice were killed at day 41 ($n=3$), 42 ($n=4$), 43 ($n=3$), and 48 ($n=1$) after infection with 10^3 to 10^6 FFU of ZIKV-Dakar. All measurements of total and motile sperm were made within 60 min of dissection of the cauda epididymis.

Testosterone and inhibin B levels. Total homogenates of testes from uninfected or ZIKV-infected mice were assayed for testosterone and inhibin B levels by radioimmunoassay as described[17] using the Research in Reproduction Ligand Assay and Analysis Core at the University of Virginia.

Fertility studies. Age-matched uninfected or ZIKV-infected wild-type C57BL/6 males (at days 7, 16 or 26 after infection, $n=4$–5 at each time point) were mated with single 8-week-old female wild-type C57BL/6 mice. Five days later, males were removed from the cage to isolate the females. Ten days later, female mice ($n=14$–15 for each group) were euthanized and evaluated for pregnancy, and the number of viable or resorbed fetuses was counted. Because sperm from mice can be obtained only at euthanasia, we were unable to perform longitudinal studies and directly correlate sperm counts after ZIKV infection with fertility rates.

Viral burden. ZIKV- or DENV-infected mice were euthanized on specific days. Testis, epididymis and other tissues were weighed and homogenized with zirconia beads in a MagNA Lyser instrument (Roche Life Science) in 200 μl PBS. All homogenized tissues from infected animals were stored at −80 °C. With some samples, viral burden was determined by plaque assay on Vero cells[35]. Sperm were subjected to three rapid freeze-thaw cycles to release infectious virus. Other samples were extracted with the RNeasy Mini Kit. ZIKV and DENV RNA levels were determined by one-step quantitative reverse transcriptase PCR (qRT–PCR) on an ABI 7500 Fast Instrument using standard cycling conditions. Viral burden was expressed on a $\log_{10}$ scale as viral RNA equivalents per g or ml after comparison with a standard curve produced using serial tenfold dilutions of ZIKV or DENV RNA as described previously[35]. For ZIKV, the following primer sets were used: 1183F: 5′-CCACCAATGTTCTCTTGCAGACATATTG-3′; 1268R: 5′-TTCGGACAGCCGTTGTCCAACACAAG-3′; and probes (1213F): 5′-56-FAM/AGCCTACCT TGACAAGCAGTC/3IABkFQ-3′.

Histology and immunohistochemistry. Tissues were collected after death and fixed overnight in 4% paraformaldehyde (PFA) in PBS. Subsequently, 5-μm-thick testis and epididymal sections from infected and uninfected mice were processed for histology by haematoxylin and eosin staining. For immunohistochemistry, the tissue sections were incubated with mouse primary monoclonal anti-CD45 (610266; BD Biosciences), anti-ETV5 (ab102010; Abcam), anti-GATA4 (ab84593; Abcam), rabbit polyclonal anti-Lin28a (3978S, Cell Signaling), rat polyclonal anti-TRA98 (ab82527; Abcam), rat polyclonal anti-F4/80 (ab6640; Abcam), or goat polyclonal anti-3β-HSD antibodies (SC-30820, Santa Cruz Biotechnology). After washing, slides were stained with Alexa Fluor 488- or, Alexa Fluor 546-conjugated goat anti-rabbit, goat anti-mouse or donkey anti-goat (1:1,000; A11008, A11081, A11030 or A11056; ThermoFisher Scientific) secondary antibodies for 1 h, and mounted with prolong gold anti-fade mount containing the nuclear counter stain, DAPI (ThermoFisher Scientific). Immunostaining was detected by confocal microscopy (Leica SPE100, Germany).

Viral RNA *in situ* hybridization. RNA ISH was performed using RNAscope 2.5 (Advanced Cell Diagnostics) according to the manufacturer's instructions. PFA-fixed paraffin-embedded tissue sections were deparaffinized by incubating for 60 min at 60 °C. Endogenous peroxidases were quenched with H_2O_2 for 10 min at room temperature. Slides were boiled for 15 min in RNAscope Target Retrieval Reagents and incubated for 30 min in RNAscope Protease Plus before probe hybridization. The probe targeting ZIKV RNA was designed and synthesized by Advanced Cell Diagnostics (Catalog #467871). Positive (targeting *plr2a* gene) and negative (targeting bacterial gene *dapB*) control probes also were obtained from Advanced Cell Diagnostics (Catalog #312471 and #310043, respectively). Tissues were counterstained with Gill's haematoxylin and visualized using bright-field microscopy.

Data analysis. All data were analysed with GraphPad Prism software. For viral burden analysis, the $\log_{10}$ transformed titres were analysed by the Mann–Whitney test or a Kruskal–Wallis one-way ANOVA. A P value of <0.05 indicated statistically significant differences.

Data availability. The datasets generated during and/or analysed during the current study are available from the corresponding author on reasonable request.

31. Lu, Q. & Lemke, G. Homeostatic regulation of the immune system by receptor tyrosine kinases of the Tyro 3 family. *Science* **293,** 306–311 (2001).
32. Esakky, P., Hansen, D. A., Drury, A. M. & Moley, K. H. Molecular analysis of cell type-specific gene expression profile during mouse spermatogenesis by laser microdissection and qRT–PCR. *Reprod. Sci.* **20,** 238–252 (2013).
33. Hansen, D. A., Esakky, P., Drury, A., Lamb, L. & Moley, K. H. The aryl hydrocarbon receptor is important for proper seminiferous tubule architecture and sperm development in mice. *Biol. Reprod.* **90,** 8 (2014).
34. Goodson, S. G., Zhang, Z., Tsuruta, J. K., Wang, W. & O'Brien, D. A. Classification of mouse sperm motility patterns using an automated multiclass support vector machines model. *Biol. Reprod.* **84,** 1207–1215 (2011).
35. Miner, J. J. *et al.* Zika virus infection during pregnancy in mice causes placental damage and fetal demise. *Cell* **165,** 1081–1091 (2016).

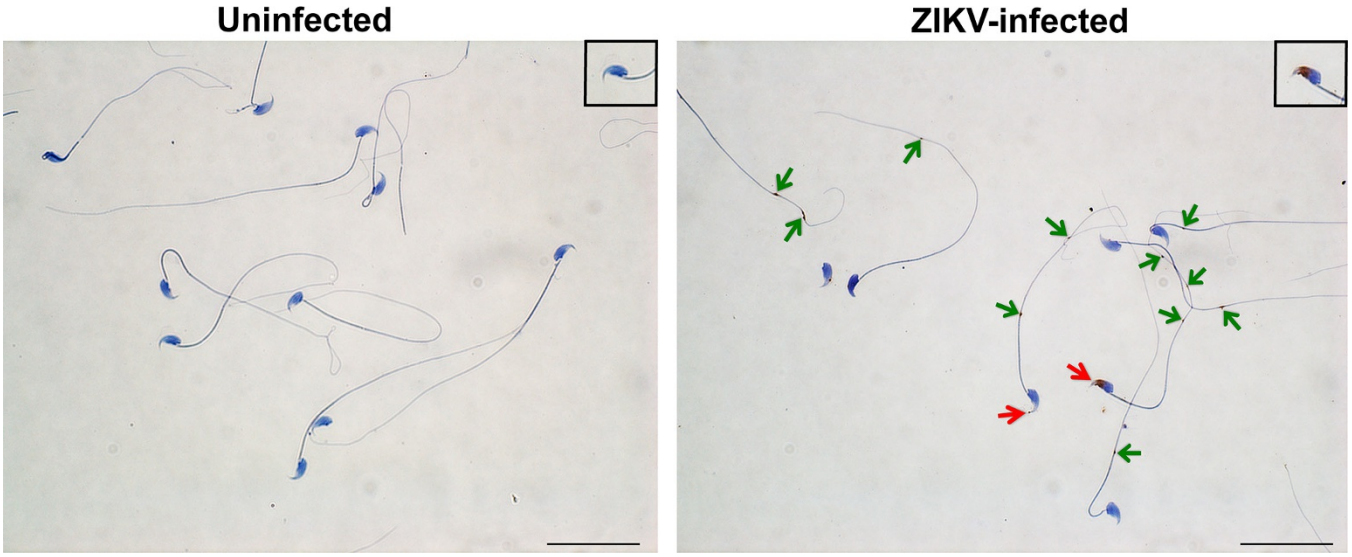

Extended Data Figure 1 | ZIKV infection of mature sperm. Mature sperm was collected from the cauda epididymis of uninfected (left) or ZIKV-infected (day 7, right) mice and processed by ISH with a ZIKV-specific probe. Staining for viral RNA is seen in the ZIKV-infected samples at the head (inset, red arrow) and in the cytoplasmic droplets (green arrows) in the sperm flagellum. Scale bar, 50 μm. Staining was quantified by microscopy: uninfected: 81 sperm counted, 0 positive for staining in head, 0 positive for staining in tail; and ZIKV-infected: 93 sperm counted, 25 (27%) positive for staining in head, 57 (61%) positive for staining in tail.

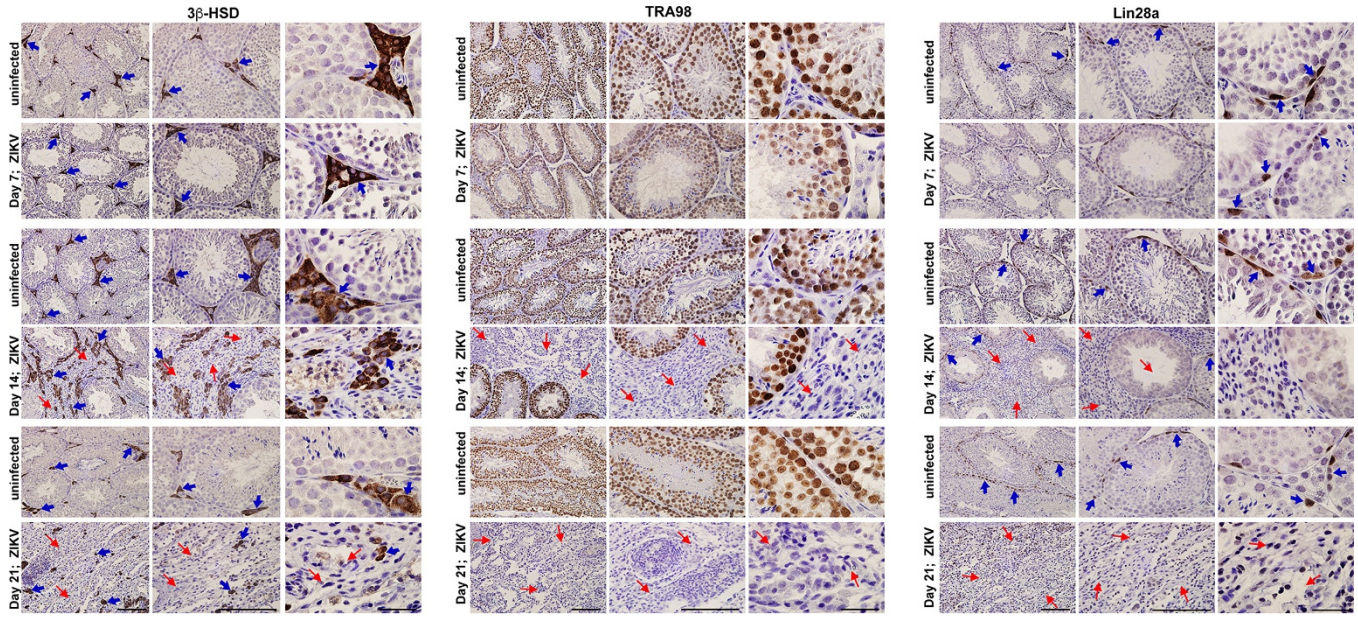

Extended Data Figure 2 | Temporal loss of cellularity in the testis after ZIKV infection. Seven-week-old wild-type C57BL/6 mice were treated with 0.5 mg of anti-Ifnar1 at day −1 before subcutaneous inoculation of mouse-adapted ZIKV-Dakar. Immunohistochemical analysis was performed on testis tissue collected from uninfected (top) or ZIKV-infected animals (days 7, 14 or 21 after infection; bottom) at 20× (left), 40× (middle) and 100× (right image) magnification. Staining was performed with antibodies against 3β-HSD (Leydig cells, top), TRA98 (germ cells, middle), and Lin28a (type A undifferentiated and type B spermatogonia, bottom). Blue arrows indicate staining of Leydig cells (top) and spermatogonial stem cells (bottom). Red arrows indicate areas of virus-induced damage and loss of tissue integrity and specific cellularity. Scale bars, 200, 200 and 50 μm for the grouping of the three sets of images.

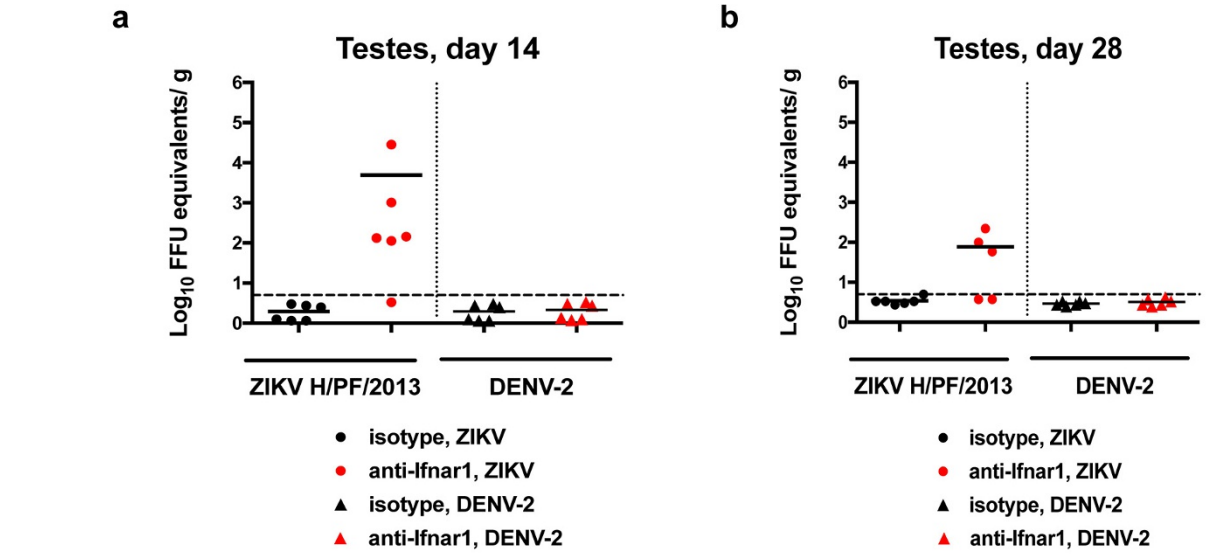

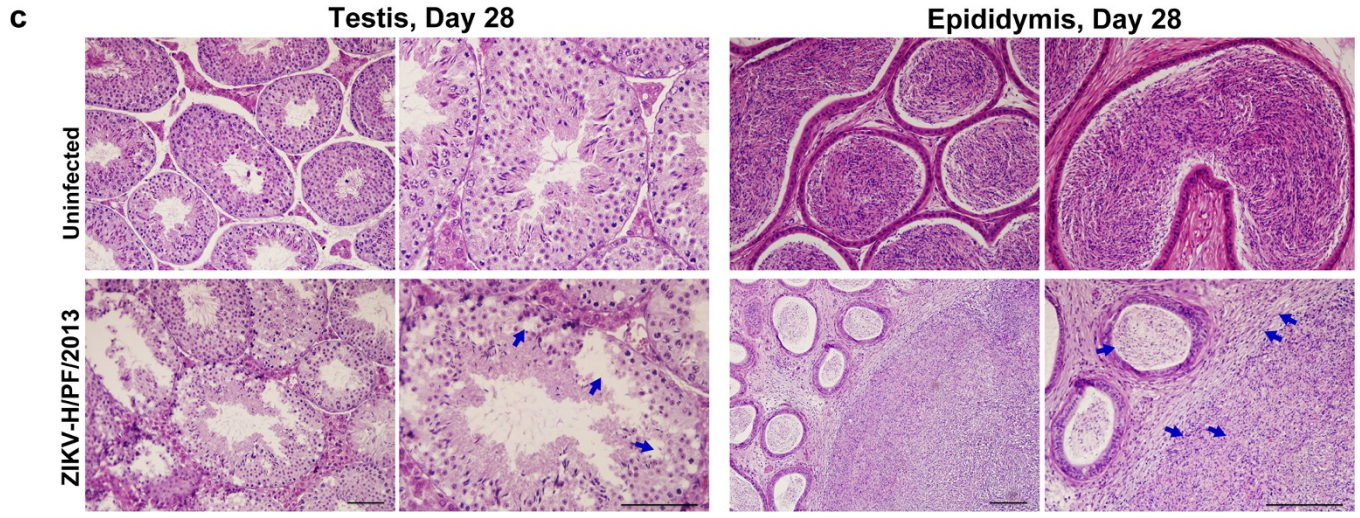

Extended Data Figure 3 | Histology of the testis at day 28 after infection with ZIKV-H/PF/2013. a, **b**, Seven-week-old wild-type C57BL/6 mice were treated with PBS or anti-Ifnar1 at day −1 before subcutaneous inoculation in the footpad with 10^3 FFU of ZIKV-H/PF/2013 or 10^6 FFU of DENV-2. Testes were collected at day 14 (**a**) or 28 (**b**) after infection and analysed for viral RNA by qRT–PCR. Results are pooled from two independent biological experiments and each symbol represents data from an individual mouse. Bars indicate mean values. **c**, Histological analysis of paraformaldehyde-fixed testis (left) and epididymis (right) collected from uninfected or ZIKV-infected animals at day 28 at 20× (left) and 40× (right) magnification. Arrows indicate loss of germ cells and vacuoles in the testis, involution of epididymal lumens with a mass of residual sperm, and thickened epithelium. The images are representative of several independent experiments. Scale bars (50 μm (left panel of each tissue) and 200 μm (right panel of each tissue)) are indicated in the bottom right corner of the panels.

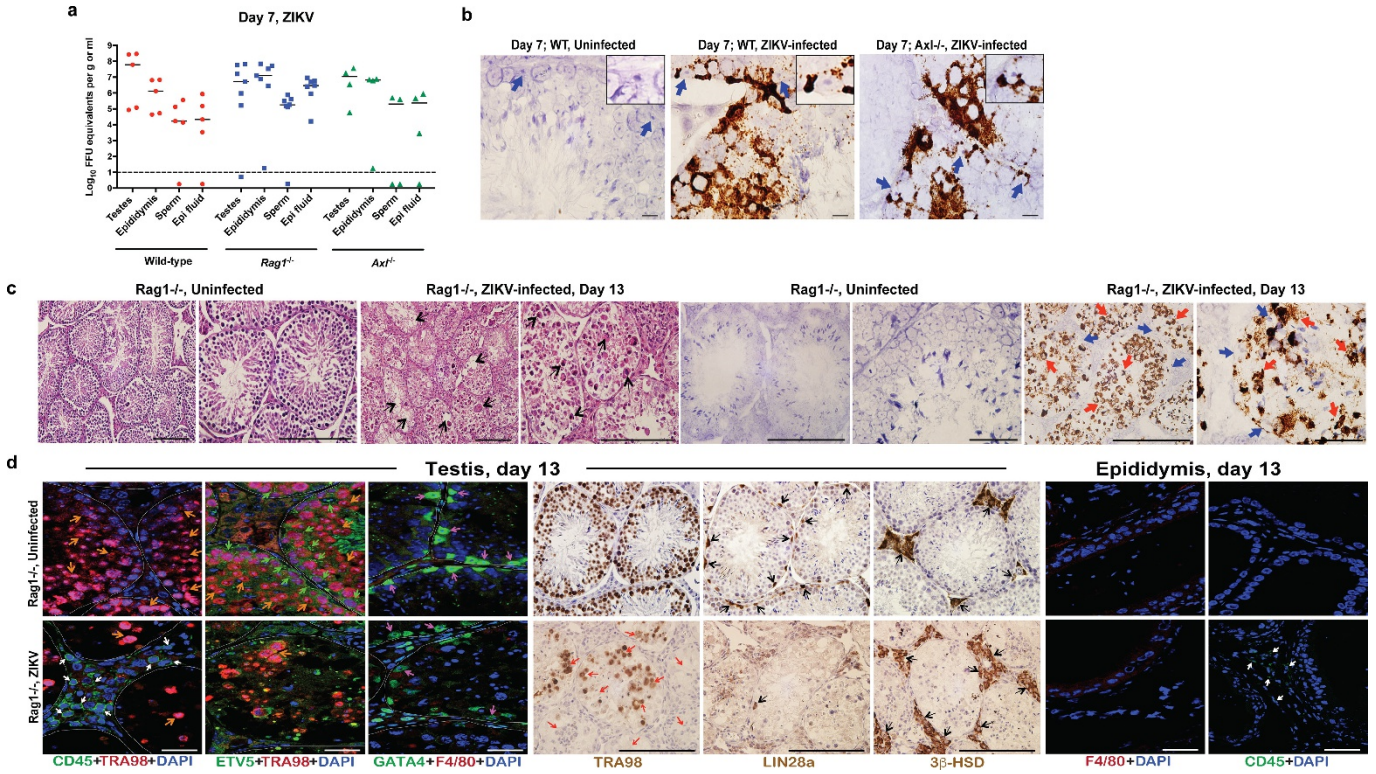

Extended Data Figure 4 | ZIKV infection of the testis and epididymis at day 7 in *Axl*$^{-/-}$ and *Rag1*$^{-/-}$ mice. Seven-week-old wild-type (WT), *Axl*$^{-/-}$ or *Rag1*$^{-/-}$ C57BL/6 mice were treated with 0.5 mg of anti-Ifnar1 at day −1 before subcutaneous inoculation in the footpad with 10^6 FFU of mouse-adapted ZIKV-Dakar. **a**, The indicated tissues were collected at day 7 after infection and analysed for viral RNA by qRT–PCR. Each symbol corresponds to data from an individual mouse and was produced from at least two independent experiments. Dashed lines indicate limit of detection of the assays. **b**, ISH of testis from uninfected or ZIKV-infected wild-type and *Axl*$^{-/-}$ mice at day 7 with a ZIKV-specific probe. Dark blue arrows indicate Sertoli cells. Inset, in sections from infected wild-type and *Axl*$^{-/-}$mice, the cytoplasm of Sertoli cells is positive for ZIKV RNA (dark brown) with signal absent from prominent nuclei and nucleoli. Scale bar, 50 μm. **c**, Histology (haematoxylin and eosin, left two) and ISH (right two) of testis from age-matched uninfected or ZIKV-infected (day 13) *Rag1*$^{-/-}$ mice at 20× (left) and 40× (right) magnification for each pair. Scale bars, 200 (the second, fourth, fifth and seventh image from the left) and 50 μm (the first, third, sixth and eighth image from the left). In haematoxylin and eosin-stained testis sections, arrows indicate loss of germ cells and presence of multi-nucleated giant and necrotic cells from ZIKV-infected *Rag1*$^{-/-}$ mice. In ISH, red and blue arrows indicate distribution of ZIKV RNA and Sertoli cells, respectively. **d**, Immunofluorescence (three left and two right) and immunohistochemistry (three middle) staining of uninfected or ZIKV-infected (day 13) testes and epididymis from *Rag1*$^{-/-}$ mice with antibodies to CD45, TRA98, ETV5, GATA4, LIN28a, 3β-HSD or F4/80 as described in Fig. 1 and Extended Data Fig. 2. Coloured arrows indicate staining for leukocytes (CD45, white), germ cells (TRA98, orange), Sertoli cells (GATA4, magenta), BTB (ETV5, green), type A undifferentiated and type B spermatogonia (Lin28a, black) and Leydig cells (3β-HSD, black). In the immunohistochemistry staining panels with TRA98, red arrows indicate dying or dead germ cells and tubules without germ cells. White lines demarcate tubules in the seminiferous epithelium. Scale bars, 200 μm for immunohistochemistry (middle three columns, for TRA98, LIN28a and 3β-HSD staining) and 50 μm for immunofluorescence (left three and right two columns). The images are representative of several different animals.

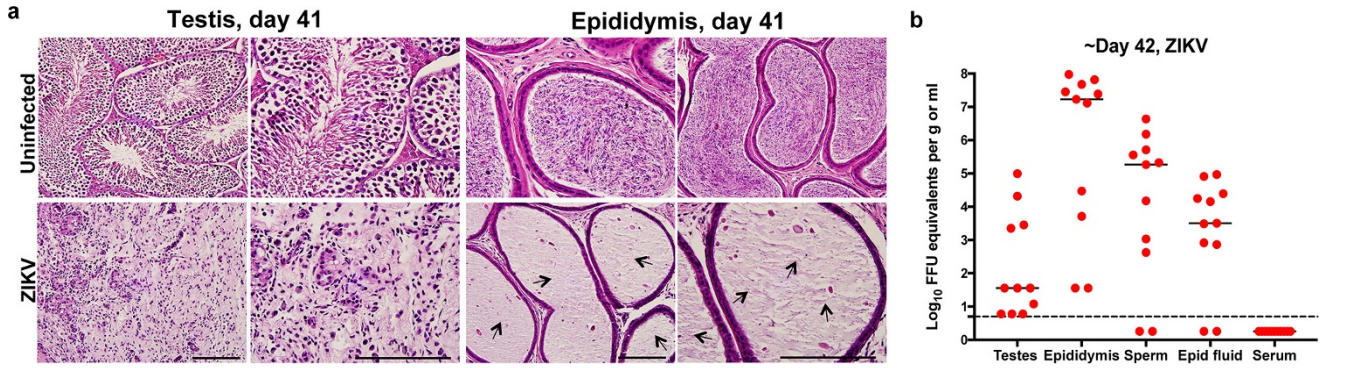

Extended Data Figure 5 | ZIKV infection of the testis and epididymis around day 42. a, Seven-week-old wild-type C57BL/6 mice were treated with anti-Ifnar1 at day −1 before subcutaneous inoculation in the footpad with 10^6 FFU of mouse-adapted ZIKV-Dakar. **a**, Testis (left) and epididymis (right) were collected at day 41 after infection or from age-matched uninfected mice, fixed with paraformaldehyde, sectioned, stained with haematoxylin and eosin, and imaged at a magnification of 20× (left) and 40× (right). Arrows show epididymal lumen void of sperm. The images are representative of sections from several independent animals. Scale bars are indicated in the bottom right corner of the panels. Scale bars, 200 μm (right columns for both testis and epididymis) and 50 μm (left columns for both testis and epididymis). **b**, The indicated tissues and cells were collected around day 42 after infection (days 41 ($n = 3$), 42 ($n = 4$), 43 ($n = 3$), and 48 ($n = 1$)) and analysed for viral RNA by qRT–PCR. Dashed line indicates the limit of detection of the assay. Results are pooled from 2–3 independent biological experiments and each symbol represents data from an individual mouse. Bars indicate median values.